Open access • Journal Article • DOI:10.1177/0278364911401441

Joint coupling design of underactuated hands for unstructured environments

Aaron M. Dollar, Robert D. Howe

Institutions: Yale University, Harvard University

Published on: 01 Aug 2011 - The International Journal of Robotics Research (SAGE Publications)

Topics: Underactuation, Revolute joint, Grippers and Contact force

Joint coupling design of underactuated hands for unstructured environments

Aaron M Dollar and Robert D Howe

The International Journal of Robotics Research 2011 30: 1157 originally published online 13 June 2011
DOI: 10.1177/0278364911401441

ijrr

The International Journal of
Robotics Research
30(9) 1157–1169

DOI: 10.1177/0278364911401441
ijr.sagepub.com
SAGE

Joint coupling design of underactuated hands for unstructured environments

Aaron M Dollar[1] and Robert D Howe[2]

Abstract

This paper examines joint coupling in underactuated robotic grippers for unstructured environments where object properties and location may not be well known. A simplified grasper consisting of a pair of two-link planar fingers with compliant revolute joints was simulated as it grasped a target object. The joint coupling configuration of the gripper was varied in order to maximize successful grasp range and minimize contact forces for a wide range of target object sizes and positions. The number of actuators was also varied in order to test performance for varying degrees of underactuation. A normal distribution of object position was used to model sensing uncertainty and weight the results accordingly. There are three main results: distal/proximal joint torque ratios of around 1.0 produced the best results, both for cases in which sensory information available for the task was poor and when sensing was good; an actuator for each gripper finger performs no better than a single actuator for both fingers; and that for good sensing, the gripper should be positioned off-center from the object, resulting in an increased lever arm and lower unbalanced contact forces on the object.

Keywords

Adaptive, robot grasping, robot hands, underactuated, unstructured environments

1. Introduction

The ability to grasp diverse objects in human settings will provide robots with the functionality to perform a wide range of tasks in homes and workplaces. However, grasping is challenging in unstructured environments, because information about the properties of target objects typically required to control the robot manipulator and end-effector are not known beforehand and must be acquired with sensing. Visual sensing can localize target objects, but cannot provide exact values for key parameters, such as object geometry and pose, and cannot provide direct information about mechanical properties, such as mass distribution, friction, and compliance.

The majority of research in robotic grasping and manipulation has attempted to address this problem through elaborate multifingered hands, combined with tactile sensing and sophisticated planning and control algorithms, and often following an anthropomorphic approach. While this methodology may provide good performance in the long term, it involves considerable systems-level complexity and significant implementation costs, and there has been little demonstrated success to date in grasping objects under the uncertainties typical of human environments.

An alternative approach uses simplified graspers incorporating passive compliance and/or adaptability in the mechanical structure of the hand. Much of the functionality of a hand can be retained by careful selection of joint compliance and coupling schemes, reducing the number of actuators and the overall complexity of the grasping mechanism. Many of these grippers are 'underactuated', with fewer actuators than degrees of freedom (e.g. Hirose and Umetani, 1978; Townsend, 2000; Laliberte et al., 2002; Dollar and Howe, 2010). These hands have also been referred to as 'adaptive' or 'self-adaptable' and can be easier to control, lighter, and less expensive than their fully actuated counterparts. See Dollar and Howe (2006) and Birglen et al. (2008) for extensive surveys of underactuated hands.

Mechanical compliance is perhaps the simplest way to allow for coupling between joints without enforcing the fixed-motion coupling relationship inherent with many gear or linkage couplings. Compliant underactuated grippers

[1]Department of Mechanical Engineering & Materials Science, Yale University, USA
[2]School of Engineering and Applied Sciences, Harvard University, USA

Corresponding author:
Aaron M Dollar, Yale University, 15 Prospect St., Becton 215, New Haven, CT 06511, USA.
Email: aaron.dollar@yale.edu

show particular promise for use in unstructured environments, where object properties are not known a priori and sensing is prone to error. Finger compliance allows the gripper to passively conform to a wide range of objects while minimizing contact forces. Passive compliance offers additional benefits in impacts, where control loop delays may lead to poor control of contact forces (Whitney, 1982; Schimmels and Huang, 1996). By reducing unwanted contact forces, compliance can also lower implementation costs by reducing the sensing and actuation required for the gripper.

There has been little work on understanding design tradeoffs in configuring underactuated hands, with most designs chosen intuitively or anthropomorphically. The designers of the 100G hand (Higashimori et al., 2005) sought to find the joint coupling that resulted in all finger links making simultaneous contact with a specific target object. The results were not only specific to the size and inertia properties of their grasper, but were only appropriate for a single target object at a specific location. Studies related to the Laval hands, alternatively, provide a more general framework for hand design. Birglen and Gosselin (2004) focus primarily on finding finger linkage configurations that generate positive forces throughout their configuration space without consideration of the effects of those forces on target objects. Laliberte and Gosselin (1998) take a similar approach and include a preliminary treatment of contact forces for one finger configuration as a function of object size and position, without discussion of how these forces are or are not appropriate for grasping.

The approach described here takes a grasp-centric view of the problem, looking at joint coupling in terms of the ability to grasp a wide range of object size and position relative to the base. We consider object size and location in order to find the best combination of joint coupling parameters to maximize the likelihood of a successful grasp, including an extensive treatment of the robustness to relative positioning error between hand and object – a parameter that can be significant in unstructured grasping tasks.

We begin this paper by describing the details of the gripper and grasping scenarios studied here. In particular, we examine the performance of a two-fingered compliant underactuated gripper as joint torque ratio and joint compliance are varied. We also examine the role of the number of actuators, contact response time, and target positioning of the hand. Finally, we provide the results of a simulation of the grasping process for a wide range of target object sizes and positions, identifying optimal joint coupling schemes for various levels of sensory information available for the grasping task.

2. Methods

In previous work, we examined the optimization of the preshape and joint stiffness of simple two-fingered grippers with passive springs in the joints for unstructured environments (Dollar and Howe, 2005). This study showed that a particular set of joint stiffnesses and rest angles could accommodate the widest range of uncertainty in object size and location. Contact forces were also minimized at approximately the same gripper configuration. In addition to simulation studies, these results were confirmed with experimental tests using a reconfigurable gripper.

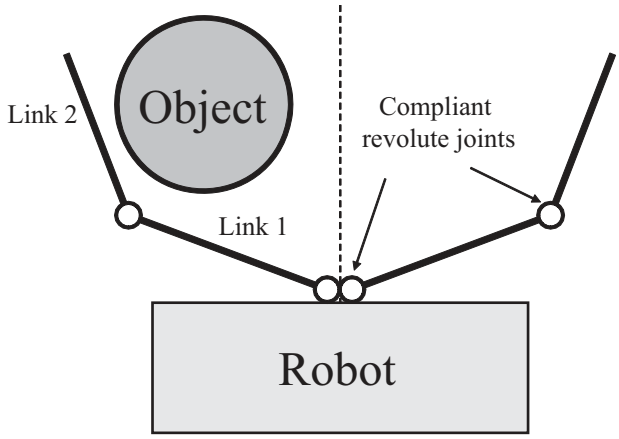

Fig. 1. A grasper mounted on a robot approaching an object to be grasped. The grasper consists of two fingers, each a two degree of freedom planar manipulator with compliant revolute joints.

Our goal in this study is to gain general insight into the advantages and disadvantages of joint coupling and specific actuation configurations under uncertainty. We thus focus on the same simple gripper with two fingers, each with two revolute degrees of freedom with springs in the joints that tend to maintain the gripper in the rest configuration (Figure 1). This gripper is perhaps the simplest configuration that is able to grasp a wide range of objects. The mechanism is the same as that used in the 100G hand (Higashimori et al., 2005) and is a planar approximation to the power-grasp configurations of the BarrettHand (Townsend, 2000), Domo hand (Edsinger-Gonzales, 2004), Obrero hand (Torres-Jara, 2005), and 4-fingered SDM hand (Dollar and Howe, 2010), among others. We use a planar analysis and assume that the links are rigid lines between joints and that each joint of the gripper includes a passive torsion spring providing a rotationally compliant joint. Our goal is to determine how variations in the joint coupling scheme and number of actuators affect the ability to grasp objects in the presence of uncertainty. For this purpose, we must define the scenario in which the grasper will operate.

2.1. Grasping scenario

To ascertain grasper performance, we must specify how it will be used to acquire objects. Note that the purpose of this study is to find the joint coupling configuration that allows the largest range of objects to be grasped under conditions of poor sensing and with as little feedback control as possible. For this reason we would like a hand

that can operate in a feed-forward mode of operation – reliably adapting to any errors in positioning without the need for complex sensing and control. Note that this is a fundamentally different problem from traditional robotic grasp analysis, where the object geometry is typically known, the robot hand has independently controllable finger joints, and the goal is to find optimal finger contact locations and commanded forces to ensure grasp stability.

This simplified control scheme enforces a limited range of potential grasping strategies. Here we investigate the most straightforward scenario based on vision and simple contact detection that makes no assumptions about object properties. In this scenario, we assume that vision has provided a rudimentary estimate of the target object location, and that the robot arm or vehicle moves straight towards this location. As the robot advances, the grasper comes into contact with the object that has unknown properties and location. The robot then stops its forward progress and the joints of the gripper are actuated to bring both fingers into contact with the object, securing the grasp. Note that in this initial study we are only interested in obtaining enveloping power grasps on the target objects for increased object stability.

Specifying the interaction between the gripper and object in unstructured environments is problematic. Ideally, the grasping process would be simulated over the entire range of object properties to determine how well each gripper design would work for any application. Object properties that are germane to the grasping process include object shape and pose on the supporting surface, as well as mechanical compliance, friction, and mass distribution. This is a high-dimensional parameter space and an exhaustive search is not practical. Instead, we make a set of assumptions that preserve the most important variations in object properties and grasper mechanical interactions. This leaves a parameter space that is still large, but where simulation is tractable to allow prediction of grasping performance.

In order to simplify the analysis, we ignore inertial effects and assume quasi-static conditions. This is plausible because the grasping process can be slow in the intended task domain, and because the finger joints are compliant and finger contact surfaces are covered with soft elastomer (Cutkosky et al., 1987; Shimoga and Goldenberg, 1992). (This does not preclude acceleration of the object due to contact forces sufficient to displace it; see below.) To simplify the geometrical calculations, the links were assumed to be simple lines through the joint axes. The object to be grasped was assumed to be circular. This is a frequent assumption in the grasping literature, because it is a reasonable approximation for many objects: it allows calculation of the typical mechanical interactions between the object and gripper while avoiding the large parameter space inherent with more elaborate shape models.

For the purposes of in-depth analysis of the mechanism, details of the actuation scheme must be specified.

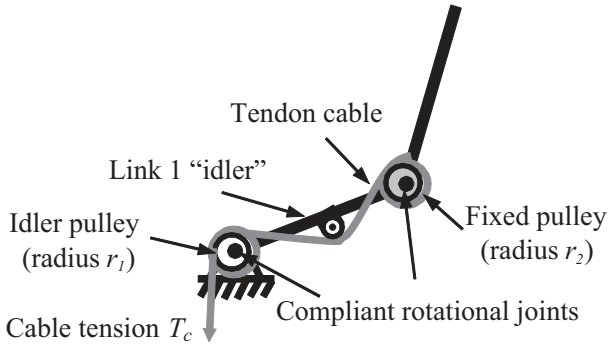

Fig. 2. Tendon and pulley arrangement for analysis purposes. Pulleys without shading are free-spinning idler pulleys that transmit no torque to their respective bases.

Table 1. Nomenclature.

Parameter	*Definition*
φ_1, φ_2	Spring rest link angles
ψ_1, ψ_2	Deflected angles
$\Delta\psi_i$	Small joint deflection due to fingerpad compliance
k_1, k_2	Joint stiffness values
k_r	Stiffness ratio (k_2/k_1)
k_s	Finger skin stiffness
τ_1, τ_2	Applied joint torque values
τ_r	Torque ratio (τ_2/τ_1)
r	Object radius
x_c	Object position from the centerline
l	Grasper link length
a_i	Distance from joint i to contact point on link i
F_T	Contact force tangential to the link surface
F_N	Contact force normal to the link surface
F_Ru	Unbalanced object force
μ	Coefficient of friction
σ	Standard deviation of object position
T_c	Cable tension
s	Cable length change
$\Delta_{\mathrm{N_j}}$	Normal fingerpad spring deflection
$\Delta_{\mathrm{T_j}}$	Tangential fingerpad spring deflection

While we employed the cable actuation scheme shown in Figure 2, this analysis applies to any method of actuation that enforces a constant distal/proximal torque ratio and has compliant joints and fingerpads, as in many underactuated hands (Table 1).

In our scheme, a tendon cable runs over a free-spinning idler pulley at joint 1 (i.e. it does not apply torque to joint 1, which allows adaptability), over another idler on link 1, and ends at a pulley on joint 2 that is fixed to link 2. Torque is applied about joint 1 via the idler located along the length of link 1, whose position and radius (along with the value of r_2) can be set in order to specify the distal/proximal torque ratio, τ_r.

Detailed steps of the grasping scenario are as follows: the grasper has some joint angle preshape of $\varphi_1, \varphi_2, \varphi_3, \varphi_4$

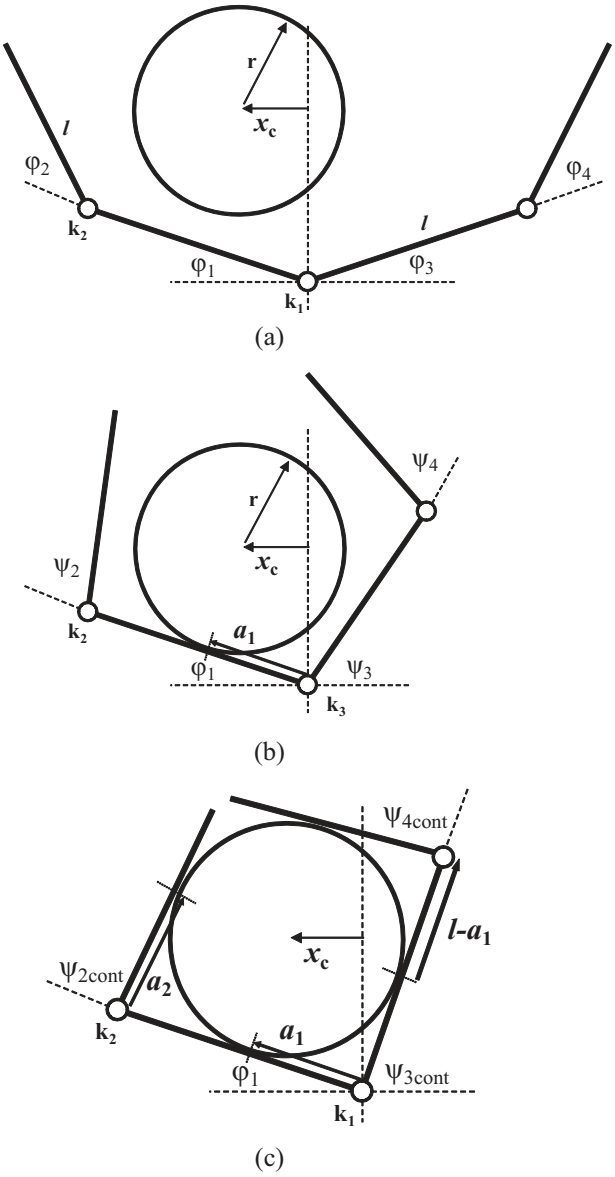

Fig. 3. Example grasping scenario with relevant terms.

(Figure 3(a)). The robot moves forward, stopping when contact is made with a circular object of radius r at position x_c from the centerline of the grasper. The gripper is then actuated, with specific behavior determined based on contact condition and actuation design, described in depth beginning in Section 2.1.1 below.

The net force applied to the target object is calculated at every time step and the grasping process is deemed unsuccessful if this force reaches a predetermined limit. For the sake of the analysis presented here, this value is set to a non-dimensional force (described later) of 1.0, approximately equivalent to the force required to displace a common canned food item ($\sim 400g$) on a typical wood surface ($\mu = \sim 0.35$) (Matheus and Dollar, 1010), given a gripper link length of 75 mm and proximal joint stiffness of 0.1 Nm/rad.

The maximum net object force and whether the grasp is successful are recorded for each combination of grasper and object parameters. Desirable gripper configurations maximize the distance from center, x_c, for which a successful grasp can be attained, while keeping contact forces as small as possible. The net force applied by the gripper to the object during acquisition should be minimized for a candidate design – the higher the value of this force, the greater the range of objects that will be displaced from their rest position during the grasping process. This parameter represents a conservative indicator of hand design quality – some objects might be successfully grasped even if sufficient force is applied to cause motion (e.g. if the object slides towards the other finger). However, motion of the target object after contact is generally undesirable, particularly in the situations considered here where object motion is not likely to be able to be compensated for due to limitations in available sensing and actuation.

2.1.1. Contact on the proximal link Due to reasons explained in the results section, the initial contact for a successful grasp is always made on the proximal link. When contact has been made, the joints of the grasper are actuated to begin to enclose the object (Figure 3(b)). At initial contact, the angle of the contact joint becomes fixed:

$$\psi_1 = \varphi_1$$

where ψ_i is the deflected angle of joint i (Table 1 summarizes the nomenclature). Grasper symmetry allows us to assume that initial contact is always on the left side (link 1).

When actuated by a joint torque τ_i, the other joints move in proportion to their stiffness, k_i:

$$\psi_i = \frac{\tau_i}{k_i} - \varphi_i, i = 2, 3, 4$$

until the respective link contacts the object (Figure 3(c)). The joint angles at contact (ψ_{icont}) can be found by

$$r \sin \psi_{3\text{cont}} - a_3 \cos \psi_{3\text{cont}} - x_c = 0$$

for joint 2, where a_3 is the lever arm length on link 3:

$$a_3 = a_1 = \frac{x_c + r \sin \psi_1}{\cos \psi_1}$$

When contact on the two inner links is made, the outer joints (2 and 4) continue to close against the object until they have made contact:

$$\psi_{2\text{cont}} = \psi_{4\text{cont}} = \pi - 2 \tan^{-1} \left(\frac{r}{l - a_1} \right)$$

This relationship comes from the symmetry of the two fingers when in complete contact with the object (Figure 3(c)) and that

$$a_2 = l - a_1$$

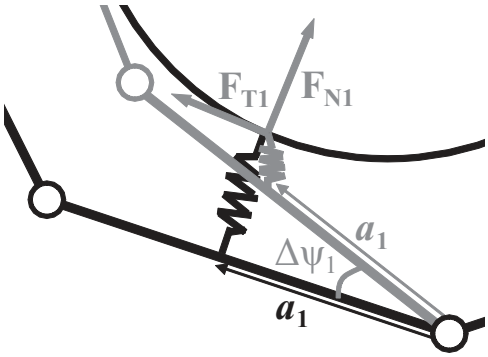

Fig. 4. Spring model of the elastic finger skin after undergoing a virtual displacement, with relevant terms.

The gripper is assumed to be covered with an elastic, high-friction skin to increase grasp stability (Cutkosky et al., 1987; Shimoga and Goldenberg, 1992). This skin is modeled as a linear spring (with stiffness k_s) positioned along the normal to the link surface with some contact friction, μ (Figure 4). As torque τ_j is increased after contact has been made, small deflections $\Delta\psi_j$ of the joint cause the spring to deflect and exert normal force F_{Nj} and tangential force F_{Tj} on the object, where

$$F_{N_j} = (\tau_j - k_j(\psi_j - \varphi_j))/a_j$$
$$\Delta\psi_j = \sin^{-1}\left(\frac{F_{N_j}}{a_j k_s}\right), j = 1, 3.$$

These small joint deflections are assumed to be insignificant displacements of the joints and do not affect grasper kinematics. They are, however, necessary to enable calculation of contact forces. The resulting tangential component of the object force is

$$F_{T_j} = a_j k_s(1 - \cos\Delta\psi_j), j = 1, 3 \quad \text{for } F_{T_j} \le \mu_s F_{N_j}$$

assuming, for simplicity, that normal skin stiffness and shear skin stiffness are equal (with stiffness k_s). For cases when the coefficient of static friction has been overcome at the contact point, $F_{T_j} = \mu_s F_{N_j}$.

Total force on the object is defined as the sum of forces at the individual contact points. For the stages of the grasping process before the outer links have made contact, this force is non-zero and must be balanced by a ground reaction force (most often due to friction) for the object to remain in equilibrium. Non-zero object force will henceforth be referred to as unbalanced object force (the non-dimensional term $F_{Ru}l/k_1$), and will be used as a quality measure that should be minimized.

2.1.2. Contact on both proximal and distal links In order to calculate the normal and tangential components of the contact forces during contact on both links of a finger, the work done by the actuator was balanced with the work done on the springs at the contact points. While we specify cable actuation to enable calculation of work, other methods of actuation can be considered in a similar way. For cable actuation with no slippage at the contact points,

$$\int_0^{s_1} T_c ds = \frac{1}{2} k_s(\Delta_{N1}^2 + \Delta_{T1}^2 + \Delta_{N2}^2 + \Delta_{T2}^2)$$

where T_c is the cable tension and s is the cable length change. These are integrated over the range from the beginning of actuation ($s = 0$) to the end of the grasp sequence ($s = s_1$, varies from case to case). Motion of the joints after contact is insignificant and does not factor into the work calculation. Δ_{Nj} and Δ_{Tj} are spring deflections normal and tangential to the surface of links $j = 1, 2$ and are related to the parameters $\Delta\psi_1$ and $\Delta\psi_2$ described in the previous section. In addition:

$$s = r_1\Delta\psi_1 + r_2\Delta\psi_2$$

and

$$T_c = \tau_2/r_2$$

where r_1 and r_2 are the pulley radii at joints 1 and 2, respectively.

For the contact point on the proximal link:

$$\Delta_{N_1} = a_1 \sin\Delta\psi_1$$
$$\Delta_{T_1} = a_1(1 - \cos\Delta\psi_1)$$

For contact on the distal link:

$$\Delta_{N_2} = \tau_2/a_2 k_s$$
$$\Delta_{T_2} = \Delta x_2 \cos(\psi_1 + \psi_2) + \Delta y_2 \sin(\psi_1 + \psi_2)$$

where Δx_2 and Δy_2 are the change in location of the contact point on the distal link due to the small joint deflections $\Delta\psi_1$ and $\Delta\psi_2$, and can be found using the forward kinematics of the mechanism:

$$\Delta x_2 = l(\cos\psi_1 - \cos(\psi_1 + \Delta\psi_1)) + a_2(\cos(\psi_1 + \psi_2) - \cos(\psi_1 + \psi_2 + \Delta\psi_1 + \Delta\psi_2))$$
$$\Delta y_2 = l(\sin\psi_1 - \sin(\psi_1 + \Delta\psi_1)) + a_2(\sin(\psi_1 + \psi_2) - \sin(\psi_1 + \psi_2 + \Delta\psi_1 + \Delta\psi_2))$$

Finally, a torque balance is performed on joint 1:

$$\tau_1 = a_1 F_{N_1} + F_{N_2} l\cos(\psi_2 + \Delta\psi_2) + F_{T_2} l\sin(\psi_2 + \Delta\psi_2)$$

where

$$F_{N_1} = k_s\Delta_{N_1}, F_{N_2} = \tau_2/a_2, \text{ and } F_{T_2} = k_s\Delta_{T_2}$$

This system of equations can be used to write the work balance and torque balance on joint 1 in terms of $\Delta\psi_1$ and $\Delta\psi_2$ and then solve them numerically. These equations also apply to links 3 and 4. In addition, a similar and simpler system of equations describes cases in which forces at a contact point overcome friction and local slip occurs.

Cases in which tip contact on one finger occurs are judged as unsuccessful grasps (Figure 5). These cases typically occur at high torque ratios (i.e. $\tau_2 >> \tau_1$) and most often result in the tip slipping and folding in towards the base joint after continued actuation, due to the large relative torque about joint 4.

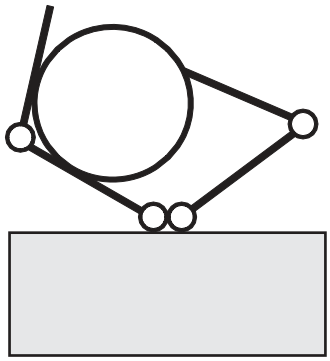

Fig. 5. Example of an unsuccessful grasp (tip contact on one link).

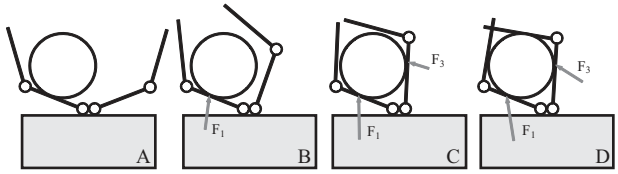

Fig. 6. Grasp scenario 1.

2.2. Specific grasping scenarios

In order to test questions related to the actuation design of the grasper, three specific grasping scenarios were studied.

2.2.1. Scenario 1 – one actuator for both fingers This actuation scenario is analogous to the scheme implemented by Hirose (Hirose and Umetani, 1978) and Ishikawa (Higashimori et al., 2005): a single actuator for the four joints (two joints on two fingers). Assuming the transmission configuration in the two fingers is the same:

$$\tau_1 = \tau_3$$

and

$$\tau_2 = \tau_4$$

In this scenario, it is assumed that the robot reacts to contact and stops immediately, with initial contact producing negligible contact forces (Figure 6(a)). When the gripper is actuated, forces are exerted at the initial contact point while the second finger is brought into contact (Figure 6(b)). Due to symmetry, the distal links on both fingers contact the object simultaneously (Figure 6(d)). The grasp is judged successful if these contacts envelop the object (enclose more than 180º of the object surface). Note that the direction of the contact forces change as the gripper is actuated, due to a squared relationship between normal and tangential contact forces due to the fingerpad springs. This relationship then becomes fixed if the friction limit has been reached and sliding occurs.

2.2.2. Scenario 1a – one actuator, further travel after contact This scenario is similar to the one above, except that

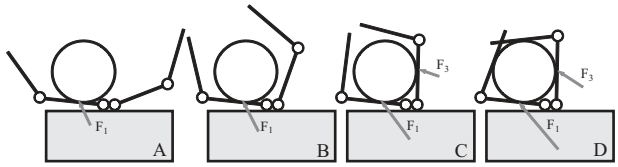

Fig. 7. Grasp scenario 1a.

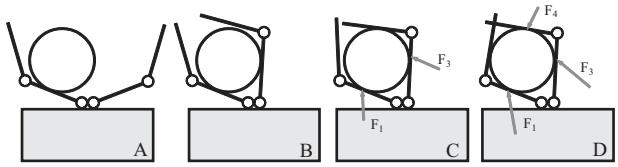

Fig. 8. Grasp scenario 2.

the grasper continues to move forward against the object for some distance after initial contact has been made, passively deflecting the contact finger and thereby exerting force on the object (Figure 7(a)). Due to sliding, the force remains on the friction cone. This scenario is studied to determine the sensitivity of the results from scenario 1 to delays in reacting to contact due to robot inertia and sensing the contact stimulus. As in scenario 1, the distal links on both fingers contact the object simultaneously (Figure 7(d)). Again, the grasp is successful if these contacts envelop the object.

2.2.3. Scenario 2 – two actuators (one per finger) In this scenario, the contact finger remains unactuated until the second finger is brought into contact with the object. As with scenario 1, the robot stops immediately at initial contact. No force is exerted on the contact link until the second finger has made contact (Figures 8(a) and (b)). Torque is then applied at an equal rate to the two proximal joints, resulting in equal forces due to symmetry (Figure 8(c)). However, the actuation of the second finger to bring link 3 into contact with the object also causes deflection of link 4, leaving it closer to the object than link 2. When the two fingers are actuated together after contact on links 1 and 3, link 4 makes contact before link 2 (Figure 8(d)).

At the point of link 4 contact, if the three contacts (links 1, 3, and 4) envelop the object (as is likely with small objects), the grasp is considered successful and the unbalanced object force $F_{\mathrm{Ru}} l/k_1$ becomes zero, since the object can no longer move in the plane. Note that for this gripper, three contacts can only geometrically enclose a circular object with radius less than $r/l = 0.5$, and only for a smaller subset of the object position x_c. For all other cases, actuation of the fingers continues until all four links are in contact and the object is enveloped.

A second possible scenario for two actuators can be considered: contact on link 1, actuate the second finger to bring link 3 into contact, immediately actuate both fingers together until link 4 makes contact, then actuate only finger 1 to bring link 2 into contact. This scenario, however, results

in identical forces to scenario 1 (one actuator), but applied in a different sequence.

2.3. Parametric analysis

The grasping scenario was simulated for a wide range of grasper parameter values, recording contact forces and the successful grasp range across a range of joint coupling configurations. The algorithm, implemented in Matlab (version 7.0.1, The Mathworks, Natick, MA), found the joint angles and object contact forces as joint torques were increased using the above system of equations. Simulation of the grasping process continued until both fingers enclosed the object.

The joint stiffnesses were applied as a ratio, since the individual magnitudes only affect the magnitude of the applied force and not the deflection behavior of the mechanism. In order to apply the actuation coupling that exists for this mechanism, individual joint torques were also applied as a ratio. Therefore, as the distal joint is brought into contact with the object, the proximal joint applies force to the object due to non-zero torque about that joint. The ratios are defined as

$$\tau_r = \frac{\tau_2}{\tau_1} = \frac{\tau_4}{\tau_3}$$

and

$$k_r = \frac{k_2}{k_1} = \frac{k_4}{k_3}$$

The motion that results when a compliant gripper is actuated is a function of both the torque and the joint stiffness. Therefore, the torque ratio was normalized by the stiffness ratio (τ_r/k_r) for an independent variable that will henceforth be referred to simply as 'torque ratio'. Note that without object contact on a given finger, this parameter reduces to

$$\frac{\tau_r}{k_r} = \frac{\psi_2 - \varphi_2}{\psi_1 - \varphi_1}$$

which is simply the flexion of the distal joint from rest over the flexion of the proximal joint from rest during free actuation (no object contact).

The object parameters x_c and r are varied to test the scenario of grasping an unfamiliar object at an unknown location. Distances and size parameters were normalized by l, the link length. The performance of the gripper for each torque ratio configuration was evaluated for normalized object radius, $r/l = \{0.1, 0.2 \ldots 0.9\}$ and object location, x_c/l, incremented by 0.0025 from the center toward the outside of the grasping range. The maximum normalized distance of the object from the centerline for which a successful enveloping grasp was attained, x_{cmax}, was recorded for each configuration. This value represents the successful grasp range.

The largest force applied to the object during the grasping process before complete object enclosure was also recorded for each tested value of object location, x_c/l. The overall goal is to determine the coupling scheme (torque ratio, τ_r/k_r) that results in the lowest unbalanced object forces $F_{Ru}l/k_1$ and the largest grasp range x_{cmax}.

It is assumed that the fingers will not interfere with each other when the links overlap, as is the case if they are slightly offset in the out-of-plane direction. The static and kinetic friction coefficients were set equal to further reduce the dimension of the parameter space. The coefficient of friction was tested at $\mu = 2$, based on previous studies that suggest high friction increases grasp stability (Cutkosky et al., 1987; Shimoga and Goldenberg, 1992). The finger skin stiffness was tested at $k_s = 1000k_1/l^2$. The results are largely insensitive to the exact value of this parameter, as it does not affect the magnitude of contact forces normal to the finger links, but serves to allow for a solution to the tangential force values to be found, which are typically much smaller than the normal forces.

The default rest angle configuration was $\varphi_1, \varphi_2 = (25, 45^\circ)$ and was based on the results of a previous study that showed this configuration allowed for the widest range of uncertainty in object size and location, while keeping contact forces low (Dollar and Howe, 2005).

3. Results

3.1. One actuator

Figure 9 shows the results of the simulation for five different object radius values under grasp scenario 1. Maximum unbalanced object force $F_{Ru}l/k_1$ was recorded as object position x_c/l and torque ratios τ_r/k_r were varied. Note that the hatched portions in the upper right of each plot are unsuccessful configurations (no grasp could be achieved), and the jagged edges are an artifact of the torque ratio and object location step size. Furthermore, areas shaded black are configurations that result in net object forces that exceed the imposed limit (i.e. $F_{Ru}l/k_1 > 1.0$).

The results show that as torque ratio is increased (for a given object position x_c/l) net contact force decreases. This result suggests that, to keep unbalanced object forces low, torque ratio τ_r/k_r should be as large as possible. However, as torque ratios increase, the position range in which an object can be successfully grasped ($\max(x_c/l)$) is decreased. This range is delimited by the outer boundary of the contour plots ($\max(x_c/l)$) in Figure 9.

This tradeoff in force versus successful grasp range can be weighed by considering the quality of the sensory information available for the grasping task. For a task in which the location of the target object is well known, the torque ratio can be large, since the gripper can be reliably centered on the object. For this case, the gripper does not need to be able to grasp objects at positions, x_c/l, far from the centerline. However, for tasks in which sensory information is poor, the positioning of the gripper is subject to large errors, requiring that the chosen torque ratio should allow for positions far from the centerline.

It should be noted that the successful grasp range results show that a successful grasp can only be achieved for object

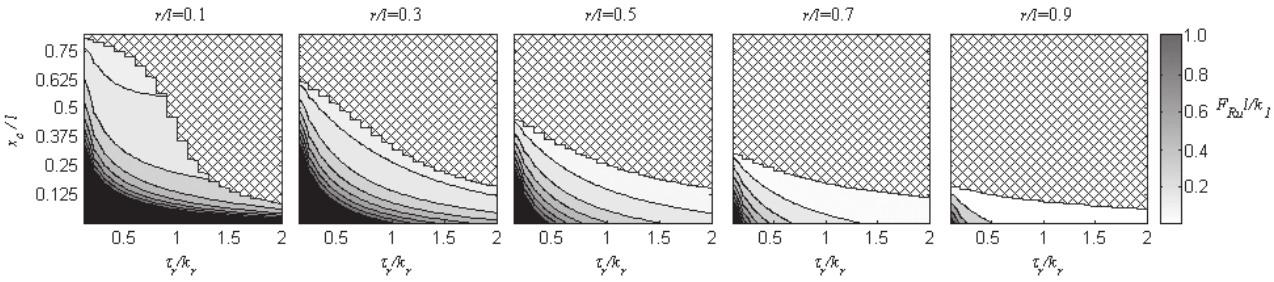

Fig. 9. Unbalanced object force ($F_{\mathrm{Ru}}l/k_1$) as object location (x_{c}/l) and size (r/l) are varied for a range of torque ratio values ($\tau_{\mathrm{r}}/k_{\mathrm{r}}$). Areas shaded black are configurations that result in net object force that exceeds the imposed limit (1.0).

positions in which initial contact is made with the inner (proximal) link. However, initial contact on the proximal link does not guarantee a successful grasp: the successful grasp range for any configuration tested is always less than the maximum object position from center (x_{c}), resulting in proximal link contact.

3.1.1. Weighted results Due to the tradeoff between large successful grasp range and low contact forces, the results of Figure 9 are further analyzed by weighting the individual data points by a normal distribution of the target object position, x_{c}/l, for a number of values of standard deviation. Different values of standard deviation of x_{c}/l correspond to different qualities of sensory information about the object prior to contact (e.g. vision) – large standard deviation corresponds to poor sensing and small standard deviation corresponds to good sensing.

Weighting functions were generated according to the normal Gaussian distribution with mean $\hat{x}_{\mathrm{t}}$ and standard deviation $\hat{\sigma}$:

$$z(\hat{x}_{\mathrm{c}},\hat{x}_{\mathrm{t}},\hat{\sigma}) = \frac{1}{\hat{\sigma}\sqrt{2\pi}} e^{\frac{-(\hat{x}_{\mathrm{c}}-\hat{x}_{\mathrm{t}})^2}{2\hat{\sigma}^2}}$$

with probability density

$$p(\hat{x}_{\mathrm{c}},\hat{x}_{\mathrm{t}},\hat{\sigma}) = \int_{-\infty}^{\hat{x}_{\mathrm{c}}} z(\hat{x'}_{\mathrm{c}},\hat{x}_{\mathrm{t}},\hat{\sigma})\, d\hat{x'}_{\mathrm{c}}$$

where $\hat{\sigma} = \sigma/l$, $\hat{x}_{\mathrm{c}} = x_{\mathrm{c}}/l$, and $\hat{x}_{\mathrm{t}} = x_{\mathrm{t}}/l$ is the 'target position' for the hand. As will be discussed below, in some cases it is better to approach the target object at some position offset from the center of the hand, therefore making it necessary to investigate object distributions with non-zero mean. Weighting functions were generated for three values of standard deviation ($\sigma/l = 1.5, 0.5, 0.1$) and target positions spanning the entire possible successful grasp range ($x_{\mathrm{t}}/l = 0, 0.05 \ldots 0.85$).

A weighted average $Q_{F_{\mathrm{Ru}}}$ of the maximum unbalanced object force over the range of object positions x_{c}/l for a given torque ratio $\tau_{\mathrm{r}}/k_{\mathrm{r}}$ was calculated using the normal distribution function:

$$Q_{F_{\mathrm{Ru}}}(\tau_{\mathrm{r}}/k_{\mathrm{r}},\hat{x}_{\mathrm{t}},\hat{\sigma}) = \frac{\int_{-x_{\mathrm{c}\,\max}(\tau_{\mathrm{r}}/k_{\mathrm{r}})}^{x_{\mathrm{c}\,\max}(\tau_{\mathrm{r}}/k_{\mathrm{r}})} F_{\mathrm{Ru}}(\tau_{\mathrm{r}}/k_{\mathrm{r}},\hat{x}_{\mathrm{c}})\, z(\hat{x}_{\mathrm{c}},\hat{x}_{\mathrm{t}},\hat{\sigma})\, d\hat{x}_{\mathrm{c}}}{\int_{-x_{\mathrm{c}\,\max}(\tau_{\mathrm{r}}/k_{\mathrm{r}})}^{x_{\mathrm{c}\,\max}(\tau_{\mathrm{r}}/k_{\mathrm{r}})} z(\hat{x}_{\mathrm{c}},\hat{x}_{\mathrm{t}},\hat{\sigma})\, d\hat{x}_{\mathrm{c}}}$$

In this quality measure on force, *smaller* values represent better performance. The limits of integration for the numerator and denominator are chosen to leave out configurations where the grasp is unsuccessful, since no reasonable force value can be assigned to them. An assigned value of zero for these configurations would artificially lower the quality measure, making the result better. Furthermore, these limits start at negative x_{cmax} (instead of zero) to take into account cases where, due to the Gaussian distribution of the object, contact might be made on one half of the hand (e.g. $-x_{\mathrm{c}}$) but be expected on the other (e.g. $+x_{\mathrm{c}}$).

To address the tradeoff that high grasp range usually leads to high contact forces, the normal probability density function was used to calculate a quality measure of the successful grasp range $Q_{X\mathrm{cmax}}$ for a given torque ratio $\tau_{\mathrm{r}}/k_{\mathrm{r}}$

$$Q_{x_{\mathrm{c}}\max}(\tau_{\mathrm{r}}/k_{\mathrm{r}},\hat{x}_{\mathrm{c}},\hat{x}_{\mathrm{t}},\hat{\sigma}) = p(x_{\mathrm{cmax}}(\tau_{\mathrm{r}}/k_{\mathrm{r}}),\hat{x}_{\mathrm{t}},\hat{\sigma}) - p(-x_{\mathrm{cmax}}(\tau_{\mathrm{r}}/k_{\mathrm{r}}),\hat{x}_{\mathrm{t}},\hat{\sigma})$$

This term represents the probability that a given torque ratio configuration will be able to successfully grasp an object with the specified target position and distribution. Under this quality measure on grasp range, *larger* values represent better performance.

Figure 10 shows an example of these weightings for a large object and large standard deviation ($r/l = 0.9, \sigma/l = 1.5$). Results for the full range of r/l and σ are not shown here because the overall trends after weighting remain the same as in Figure 9.

In order to provide a measure of the tradeoffs between minimizing force and maximizing grasp space, the quotient of the two quality measures can be analyzed:

$$Q(\tau_{\mathrm{r}}/k_{\mathrm{r}},\hat{x}_{\mathrm{c}},\hat{x}_{\mathrm{t}},\hat{\sigma}) = \frac{Q_{x_{\mathrm{c}}\max}(\tau_{\mathrm{r}}/k_{\mathrm{r}},\hat{x}_{\mathrm{c}},\hat{x}_{\mathrm{t}},\hat{\sigma})}{Q_{F_{\mathrm{Ru}}}(\tau_{\mathrm{r}}/k_{\mathrm{r}},\hat{x}_{\mathrm{c}},\hat{x}_{\mathrm{t}},\hat{\sigma})}$$

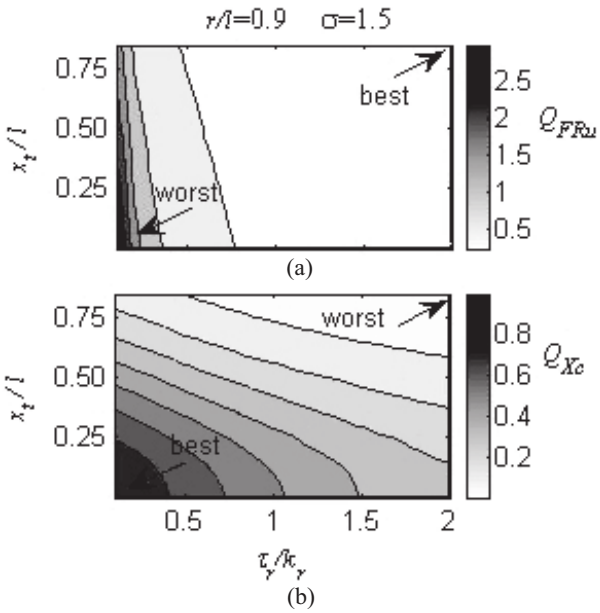

Fig. 10. Force quality (a) and successful grasp range quality for a large object and poor sensing ($r/l = 0.9, \sigma/l = 1.5$).

By calculating an overall quality measure in this way, we are using the force quality measure as a weighting function on the probability of successful grasp. Note that this relative weighting of $Q_{F\mathrm{Ru}}$ and $Q_{X\mathrm{cmax}}$ is somewhat arbitrary, but gives some sense of the tradeoffs between force and successful grasp range. Weighting these parameters differently will give different results and might be varied based on the specific scenario to be studied.

Figure 11 shows Q across a wide range of object size ((a)–(c): $r/l = 0.1, 0.5, 0.9$) and a normalized average (d) over all tested object sizes ($r/l = 0.1, 0.3, 0.5, 0.7, 0.9$) for three different standard deviations (columns: $\sigma/l = 1.5, 0.5, 0.1$). In each plot, the horizontal axes are torque ratio $\tau_\mathrm{r}/k_\mathrm{r}$, the vertical axes are gripper target position x_t/l, and the contours are the overall quality Q, with darker areas having *higher* quality.

The normalized average (Figure 11(d)) is the average over the five object sizes after each has been normalized by their individual maximum value. The magnitudes of Q across object size are not comparable, and a direct average would not give equal weighting to all objects. Alternatively, this quantity could be replaced by an average weighted by the distribution of the expected object size, if known.

According to these results, for poor sensing (large standard deviation in object position, $\sigma/l = 1.5$ – Figure 11(d), right-hand plot), a hand should be designed with a torque ratio of approximately $\tau_\mathrm{r}/k_\mathrm{r} = 1$. While this is the optimum when averaged across object size, there is high quality around this value across the entire range of object sizes. These results also show that targeting the object in the center ($x_\mathrm{t}/l = 0$) gives the best performance for poor sensing, except for the smaller objects, which are better grasped slightly off-center ($x_\mathrm{t}/l \approx 0.4$ for $r/l = 0.1$).

As the standard deviation decreases (better sensing), the optimum torque ratio generally shifts towards higher $\tau_\mathrm{r}/k_\mathrm{r}$ and becomes more sensitive to object size. Note that the results for $\sigma/l = 0.1$ are nearly identical to the unweighted data (Figure 9), as would be expected.

Based on these results, it is often best to target the object off-center ($x_\mathrm{t}/l > 0$), particularly for smaller objects, thereby increasing the distance of the contact location (lever arm) from the base joint and lowering contact forces for a given joint torque. For tasks in which excellent sensing is available, the best positioning strategy is to target the location resulting in the lowest forces that also results in a successful grasp. This location is near the upper boundary (large x_t/l) of the contours in Figure 9. However, the torque ratio resulting in the best performance is less obvious. The averaging done in Figure 10(b) makes less sense for scenarios with good sensing than for poor sensing, since the target location need not be predetermined and can be decided based on the sensed object size. *In this case, the best torque ratio should not be a function of* x_t/l.

Figure 12 shows the maximum Q across all x_t/l as torque ratio is varied, normalized to the maximum across torque ratio, for three objects (solid lines: $r/l = 0.1, 0.5, 0.9$), the average of the normalized curves across all objects (dotted line), and the minimum Q across the normalize maxima across all objects (dashed line). Note that the 'steps' in the curves are artifacts of the discrete values of object location and applied joint torque. As in Figure 9, the results show that a lower torque ratio should be used with small objects ($\tau_\mathrm{r}/k_\mathrm{r} \approx 0.4$) and a large torque ratio for large objects ($\tau_\mathrm{r}/k_\mathrm{r} > 2.0$). The average across object size (dashed line) shows that any value of $\tau_\mathrm{r}/k_\mathrm{r} > 0.5$ performs well.

However, by taking the average, bad performance for one object (e.g. $\tau_\mathrm{r}/k_\mathrm{r} = 2.0$ for $r/l = 0.1$) is sometimes balanced by good performance by another object (e.g. $\tau_\mathrm{r}/k_\mathrm{r} = 2.0$ for $r/l = 0.9$). By looking at the minimum quality across object size for each value of torque ratio and designing for the 'best worst case', acceptable performance across all objects is achieved, rather than a mixture of good and poor performance. In this case, a torque ratio of around $\tau_\mathrm{r}/k_\mathrm{r} = 1.0$ ensures that overall quality for all object sizes is above 50% of the maximum for that object. This value is within the maximum range of the average as well.

3.1.2. Stop-delay sensitivity In the previous scenario, the grasper is actuated at the instant of initial contact with the target object. No further travel of the robot vehicle occurs. However, sensing delays and inertia in a real task require time for the robot to react to contact and come to a stop. We model these effects as forward travel after contact with the object (grasp scenario 1a), resulting in passive deflection of the compliant joints of the gripper, and contact force prior to actuation.

Figure 13 shows the product quality measure for a large object under poor sensing ($r/l = 0.9, \sigma/l = 1.5$) for two

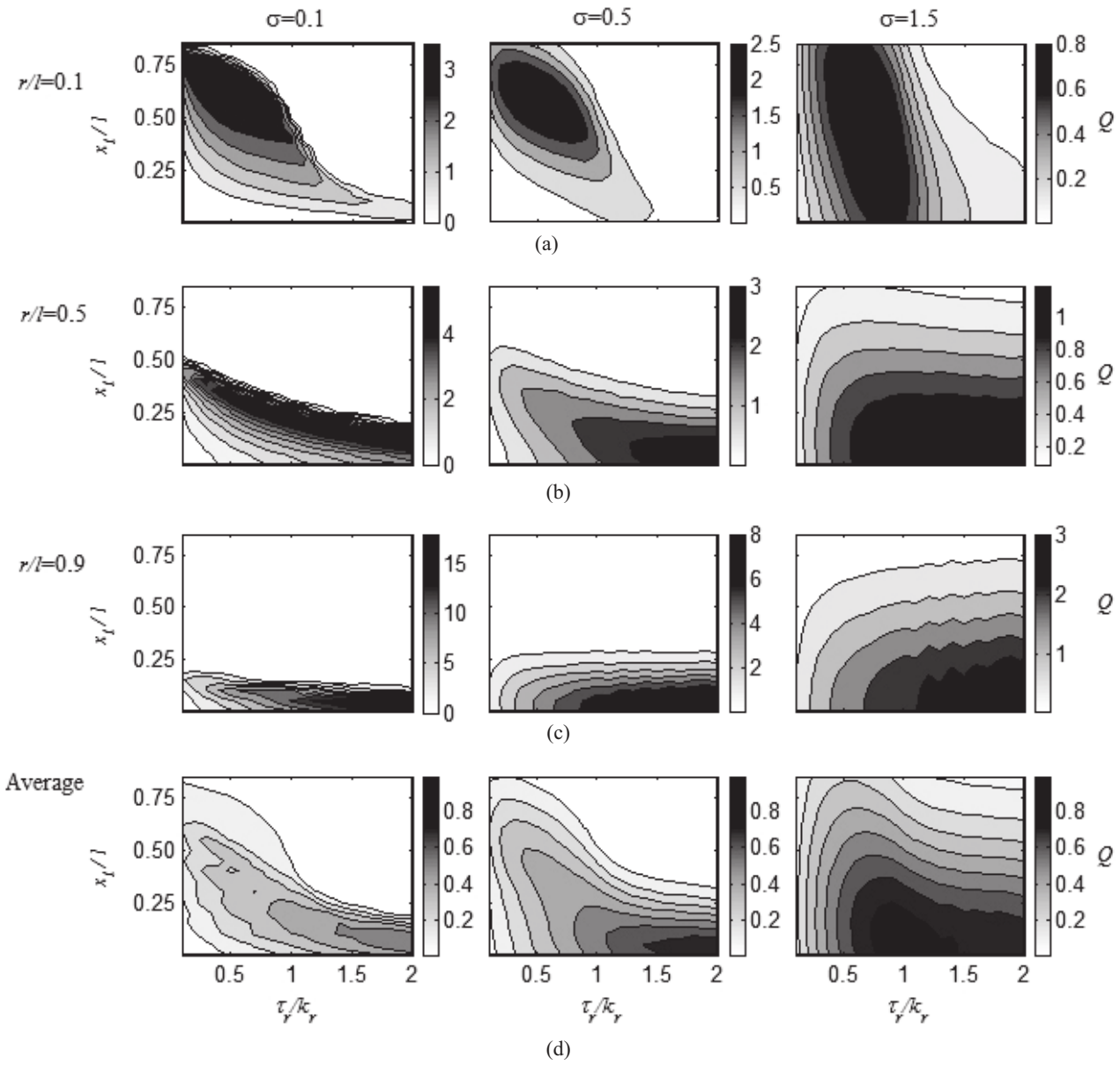

Fig. 11. Overall quality Q as object size (r/l – rows) and distribution (σ/l – columns) are varied for a range of torque ratio values (τ_r/k_r – horizontal axes) and target positions (x_t/l – vertical axes). Note that each plot has a different scaling of the contours to show detail.

cases: a large amount of forward travel occurring after contact was made ($y/l = 0.09$ across the entire successful grasp range), and no forward travel (stop on initial contact – scenario 1). Note that the scale of the contours is different between the two plots.

Since forward travel after contact leads to large contact forces due to the passive joint stiffness, Q decreases with forward travel. However, the optimum torque ratio does not vary much with forward travel after contact.

Note that near the centerline (x_c/l is small), smaller objects will hit the stiff grasper base joint after just a small amount of forward travel after contact, lending further weight to the idea that grasping the object off-center is often a better strategy.

3.2. Two actuators

To investigate whether there is any advantage to using two actuators (one per finger), grasp scenario 2 was investigated. Figure 14 shows the unweighted results of this simulation. The successful grasp ranges for this scenario (boundary of the contour plots) are identical to scenario 1 (Figure 9). However, the force results are different. For the smaller objects ($r/l = 0.1, 0.3$), most of the forces are smaller than the single-actuator scenario, resulting in better overall quality Q (not shown).

For medium and large objects ($r/l = 0.5, 0.7, 0.9$), the forces are significantly larger than for a single actuator (Figure 9), resulting in lower Q. For these cases, there are lower forces exerted on link 1 and higher forces exerted on

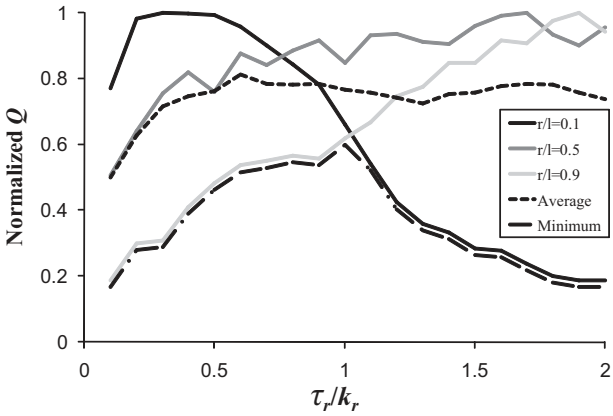

Fig. 12. Normalized overall quality for $\sigma/l = 0.1$ for three object sizes ($r/l = 0.1, 0.5, 0.9$) and an average across objects.

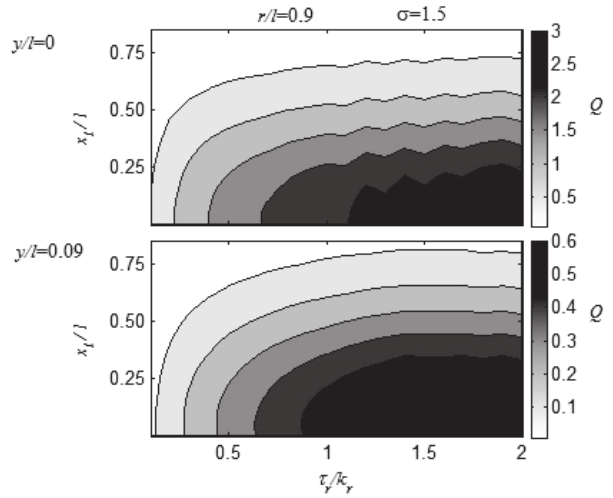

Fig. 13. Overall quality for a large object and standard deviation ($r/l = 0.9, \sigma/l = 1.5$) when the robot travels forward some distance y/l after initial contact.

link 4. For these objects, four contact points are needed to envelop the object, requiring that link 4 applies force as the final link (link 2) is being brought into contact. Depending on the torque ratio and contact locations (lever arm), these forces are often much larger than the forces on links 1 and 3, and may result in a large unbalanced object force. The symmetry inherent with scenario 1 necessitates that the object is enveloped when links 2 and 4 make simultaneous contact, and therefore forces applied at these links do not contribute to the unbalanced object force.

These results show that for multi-purpose grippers (intended to grasp a wide range of objects) and grippers specialized for medium and large objects with respect to the gripper size (which makes sense for a 'specialized' gripper), a design consisting of one actuator *per finger* of the gripper does not perform any better than a single actuator for the two fingers, due to the enforced symmetry in the grasping task with one actuator.

4. Discussion

The very nature of unstructured environments hinders full utilization of a complex, fully actuated hand. In order to effectively use the added degrees of actuation, an accurate model of the task environment is necessary. This model can be built from real-time sensing, but this requires a substantial sensor suite, signal processing system, and control algorithms. While there has been considerable progress on the components of such a system, reports of successful experimental implementation in unstructured environments have been few to none. While this approach may eventually succeed in providing excellent performance, the complex sensing and control required will also entail high implementation costs and frequent hardware failures. A gripper with a reduced number of actuators is simpler to use and less expensive to develop, and is more appropriate for the present state of the art.

Towards this goal, this paper evaluated a simple, two-fingered underactuated gripper as it was actuated after contact with a target object. Unlike the few other systematic design studies that have addressed underactuated hand design (e.g. Laliberte and Gosselin, 1998; Birglen and Gosselin, 2004; Higashimori et al., 2005), we consider object size and location in order to find the best design to maximize the likelihood of a successful grasp. We optimize the performance of the gripper in an 'unstructured environment' by varying the joint coupling configuration and number of actuators of the gripper in order to find configuration with the maximum successful grasp range while minimizing contact forces for a wide range of target object sizes and positions. We showed that a single actuator for both gripper fingers performs just as well as one actuator per finger, in terms of successful grasp range and unbalanced contact forces. For a single actuator, distal:proximal joint torque ratios of around 1:1 produced the best results both for cases in which sensory information available for the task was poor and for cases in which sensory information available for the task was good.

Another interesting observation from this investigation is that, for the scenarios considered, it is often better to grasp the object some distance away from the centerline, that is, approach the object off-center from the middle of the grasper. Contacting the object towards the center of the grasper results in high forces due to small lever arm on the proximal joint, less allowable travel forward after contact before the joint limits are reached, and a less stable enveloping grasp due to a smaller amount of object enclosure. However, in the presence of uncertainty in the object properties, approaching the object off-center runs the risk of the object being outside of the successful grasp range, particularly for large objects. An interesting possible line of inquiry is whether an asymmetric hand design is advantageous in the scenarios in which an off-centered approach is appropriate.

A number of key assumptions were made in order to make the study tractable. The requirement of an enveloping grasp is appropriate, since the grasping environment is

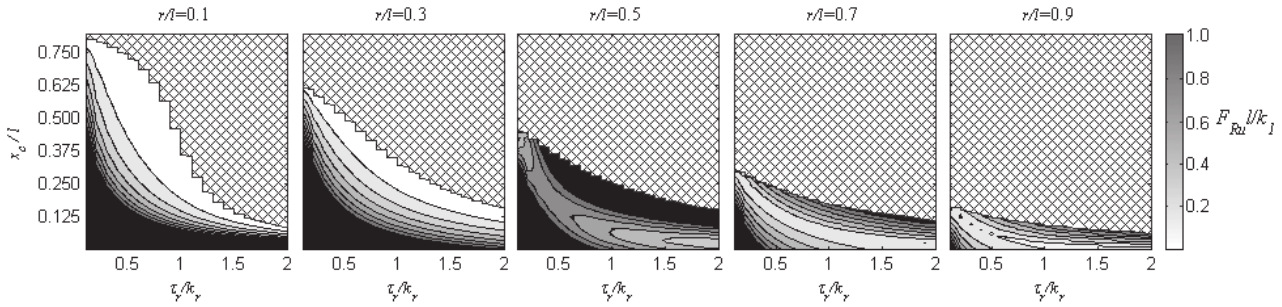

Fig. 14. Unbalanced object force ($F_{\mathrm{Ru}}l/k_1$) as object location (x_{c}/l) and size (r/l) are varied for a range of torque ratio values ($\tau_{\mathrm{r}}/k_{\mathrm{r}}$) for two actuators (scenario 2). Areas shaded black are configurations that result in net object force that exceeds the imposed limit (1.0).

uncertain, but in practice force closure is sufficient for a stable grasp. Evaluating the gripper performance for only circular objects is also simplistic; however, preliminary evaluation of other object shapes suggests that the optimum configurations also apply to a range of convex objects. The choice of a large value for the coefficient of friction can also be debated, although preliminary studies suggest it does not have a large effect on the results. Prior work investigated the role of friction during reaching, before grasp initiation (Dollar and Howe, 2005).

Preliminary experimental evaluation of a hand designed based on the results of this study demonstrates the ability to reliably grasp 5 cm-scale objects ($r/l = 0.4$) in the presence of positioning error of up to 100% of the object size and 10 cm-scale objects ($r/l = 0.8$) in the presence of positioning error of up to 33% of the object size, while keeping acquisition contact forces low (Dollar and Howe, 2010). These results lend weight to the acceptability of the assumptions made in this study by demonstrating robust grasping of real, three-dimensional objects under typical grasping conditions with simplified sensing and control.

While we employed a specific actuation scheme in this study (i.e. tendon-based) in order to allow for analysis of the mechanism, the results of this study apply to any method of actuation that enforces a constant distal/proximal torque ratio. The weighting scheme used in this study, while providing a general framework for addressing the tradeoffs between successful grasp range and contact force, uses relative weightings that can be specialized for a given application. Our choice in specific weightings makes sense for the conditions that we are most interested in: grasping a broad range of target objects in the presence of large uncertainties in location and object properties. However, these may not be best for other scenarios. For instance, for a task in which target objects are known to be massive, choosing a coupling scheme that weights successful grasp range much larger than low contact forces may be more appropriate.

This initial study examined perhaps the simplest grasping scenario under somewhat limiting assumptions, but demonstrated that a simple actuation scheme promises good performance. This design approach can be readily extended to other grasping scenarios and a broader parameter space, albeit at the cost of greater computational complexity. In particular, it will be useful to investigate the use of very simple sensor-based control. This could allow, for example, repositioning of the hand after initial contacts in order to center it on the inferred object location (Dollar et al., 2010). The resulting symmetry might serve to lower net forces as the fingers are closed to enable stable grasping of lightweight or top-heavy objects. Similar simple sensing and control algorithms could also enable grasping of concave objects. By progressing from the simplest scenario considered here to more elaborate grasping systems, it will be possible to characterize the tradeoffs between gripper complexity and grasping performance in unstructured environments.

Funding

This work was supported by the Office of Naval Research (grant number N00014-98-1-0669).

Conflict of interest

The authors declare that they have no conflicts of interest.

Acknowledgment

A preliminary version of parts of this paper was presented at the American Society of Mechanical Engineers (ASME) Mechanisms and Robotics Conference, part of the ASME International Design Engineering Technical Conferences (IDETC), Philadelphia, PA, USA, September 2006.

References

Birglen L and Gosselin C (2004) Kinetostatic analysis of underactuated fingers. *IEEE Transactions of Robotics and Automation* 20(2): 211–221.

Birglen L, Laliberte T and Gosselin C (2008) *Underactuated Robotic Hands*. New York: Springer.

Cutkosky MR, Jourdain JM and Wright PK (1987) Skin materials for robotic fingers. In: *Proceedings of the 1987 IEEE International Conference on Robotics and Automation*, pp. 1649–1654.

Dollar AM and Howe RD (2005) Towards grasping in unstructured environments: grasper compliance and configuration optimization. *Advanced Robotics* 19(5): 523–544.

Dollar AM and Howe RD (2006) Joint coupling design of underactuated grippers. In: *Proceedings of the 2006 ASME International Design Engineering Technical Conferences (IDETC), Mechanisms and Robotics Conference*.

Dollar AM and Howe RD (2010) The highly adaptive SDM hand: design and performance evaluation. *The International Journal of Robotics Research* 29(5): 585–597.

Dollar AM, Jentoft L, Gao JH and Howe RD (2010) Contact sensing and grasping performance of compliant hands. *Autonomous Robots* 28(1): 65-75.

Edsinger-Gonzales A (2004) Design of a compliant and force sensing hand for a humanoid robot. In: *Proceedings of the 2004 International Conference on Humanoid Manipulation and Grasping (IMG04)*.

Higashimori M, Kaneko M, Namiki A and Ishikawa M (2005) Design of the 100G capturing robot based on dynamic preshaping. *The International Journal of Robotics Research* 24(9): 743–753.

Hirose S and Umetani Y (1978) The development of soft gripper for the versatile robot hand. *Mechanism and Machine Theory* 13: 351–359.

Laliberte T, Birglen L and Gosselin C (2002) Underactuation in robotic grasping hands. *Machine Intelligence & Robotic Control* 4(3): 1–11.

Laliberte T and Gosselin CM (1998) Simulation and design of underactuated mechanical hands. *Mechanism and Machine Theory* 33(1): 39–57.

Matheus K and Dollar AM (2010) Benchmarking grasping and manipulation: properties of the objects of daily living. In: *Proceedings of the 2010 IEEE International Conference on Intelligent Robotics and Systems (IROS)*.

Schimmels JM and Huang S (1996) A passive mechanism that improves robotic positioning through compliance and constraint. *Robotics and Computer-Integrated Manufacturing* 12(1): 65–71.

Shimoga KB and Goldenberg AA (1992). Soft materials for robotic fingers. In: *Proceedings of the 1992 IEEE International Conference on Robotics and Automation*, pp. 1300–1305.

Torres-Jara E (2005). Obrero: a platform for sensitive manipulation. In: *Proceedings of the 2005 IEEE-RAS International Conference on Humanoid Robots*, pp. 327–332.

Townsend WT (2000) The BarrettHand Grasper - Programmably Flexible Part Handling and Assembly. *Industrial Robot – An International Journal* 10(3): 181-188.

Whitney DE (1982). Quasi-static assembly of compliantly supported rigid parts. *Journal Dynamic Systems, Measurement, and Control* 104: 65–77.